Journal of Asian Earth Sciences 177 (2019) 240–249

Contents lists available at ScienceDirect

Journal of Asian Earth Sciences

journal homepage: www.elsevier.com/locate/jseaes

Full length article

Luminescence chronology and palaeoenvironmental significance of limnic relics from the Badain Jaran Desert, northern China

Tianyuan Chen[a,b,f,*], Zhongping Lai[c], Siwen Liu[d,i,*], Yixuan Wang[a,b,f], Zhen-ting Wang[e], Xiaodong Miao[h], Fuyuan An[g], Lupeng Yu[h], Fengqing Han[a,b]

[a] Key Laboratory of Comprehensive and Highly Efficient Utilization of Salt Lake Resources, Qinghai Institute of Salt Lakes, Chinese Academy of Sciences, Xining 810008, China
[b] Key Laboratory of Salt Lake Geology and Environment of Qinghai Province, Qinghai Institute of Salt Lakes, Chinese Academy of Sciences, Xining 810008, China
[c] Institute of Marine Science, Shantou University, Shantou 515063, China
[d] National Research Center for Geoanalysis, Beijing 100037, China
[e] Cold and Arid Regions Environmental and Engineering Research Institute, Chinese Academy of Sciences, Lanzhou 730000, China
[f] University of Chinese Academy of Sciences, Beijing 100049, China
[g] Qinghai Provincial Key Laboratory of Physical Geography and Environmental Processes, School of Geographical Science, Qinghai Normal University, Xining 810008, China
[h] Shandong Provincial Key Laboratory of Water and Soil Conservation and Environmental Protection, School of Resource and Environmental Sciences, Linyi University, Linyi 276000, China
[i] Key Laboratory of Eco-geochemistry, Ministry of Natural Resources, Beijing 100037, China

ARTICLE INFO

Keywords:
Badain Jaran Desert
Limnic relics
Late Quaternary
K-feldspar pIRIR dating
Quartz OSL dating

ABSTRACT

The Badain Jaran Desert in northern China is well known for the highest mega-dunes on Earth and unique alternating megadune–lake landform, and various formation mechanisms have been proposed. Although the relics of interdune lakes are generally considered as good palaeoenvironmental records, their evolutions and relevance to paleoenvironment change are poorly understood due to limited age control. In this study, quartz optically stimulated luminescence (OSL) and K-feldspar post-infrared infrared stimulated luminescence (pIRIR) were used to establish a chronological framework for limnic relics in order to reconstruct the evolution of interdune lakes. Our results indicate that limnic relics were deposited in MIS 5 and MIS 1, due to a lake level transgression and humid environmental condition. During the Holocene, humid conditions occurred at early to middle Holocene, immediately preceded and followed by aridity. The last 600 years have been characterized by high rates of aeolian activity. Based on field observation and luminescence ages, we propose that climate fluctuations since the Late Pleistocene have played a pivotal role in the formation of the unique landform assemblages.

1. Introduction

The Badain Jaran Desert (BJD) in northern China contains the highest megadunes on Earth and a unique alternating megadune–lake landscape. At the present day, the region is in the transitional zone between the Asian summer monsoon and the Westerlies, and the desert environment is influenced by both wind systems (Chen et al., 2008). Several mechanisms have been proposed for the formation of the alternating megadune–lake landscape, including control of underlying morphology (Lou, 1962; Sun and Sun, 1964; Tan, 1964), climate changes which leads to fixation, reactivation and ultimate formation of megadunes (Wang, 1990; Dong et al., 2004), groundwater which maintains the mega-dune landscape (Chen et al., 2004a), and wind erosion to form interdune lake basins during arid periods (Wang et al., 2016b). The influence of climate change has been studied extensively in recent years and it is now regarded as one of the key megadune–lake formation factors (Yang, 2000, 2001; Yang and Williams, 2003; Yang et al., 2003, 2010; Li et al., 2015b, 2015c; Wang et al., 2015, 2016a; Liu et al., 2016).

Previous chronological studies have shown that the climate of the BJD fluctuated at both orbital and millennial scales since the Late Pleistocene (Fig. 1). Yan et al. (2001a, 2001b, 2001c) dated a fossilized

* Corresponding authors at: Key Laboratory of Comprehensive and Highly Efficient Utilization of Salt Lake Resources, Qinghai Institute of Salt Lakes, Chinese Academy of Sciences, Xining 810008, China (T. Chen). National Research Center for Geoanalysis, Beijing 100037, China (S. Liu).
E-mail addresses: chen.tianyuan@foxmail.com (T. Chen), siwenzliu@126.com (S. Liu).

https://doi.org/10.1016/j.jseaes.2019.03.024
Received 10 October 2018; Received in revised form 24 March 2019; Accepted 31 March 2019
Available online 02 April 2019

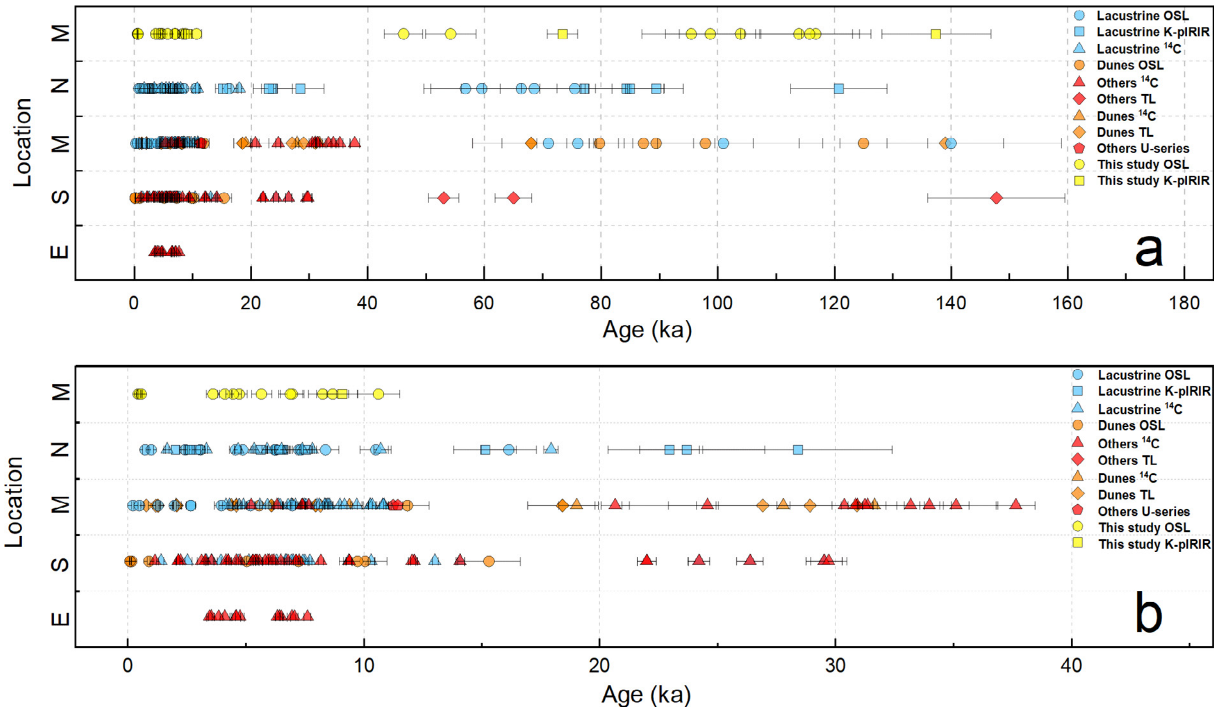

Fig. 1. Summary of published chronological data (including the OSL and K-pIRIR ages of the current study) of the Badain Jaran Desert and comparison with regional climate records over the past 150 ka (a) and 40 ka (b). The records mainly from east (E), south (S) and north (N) of the Badain Jaran Desert (M). More detailed information please see Table S1 in the supplementary materials.

dune near the west edge of the desert and a megadune in the southeast of the desert using thermoluminescence (TL). They proposed that the fossilized dune was present before the last interglacial period while the megadune formed during the last glacial period (based on six TL ages). Yang (2000) radiocarbon dated several calcareous cementation layers and cemented plant roots in megadunes and identified four more humid climate stages in the BJD in the last 31 ka. Combined with more detailed studies, including TL and radiocarbon dating of lacustrine and aeolian sediments, the results indicate that the moisture source of the more humid climate at ca 31 and 19 k ^{14}C a BP was from the westerlies, while the more humid climate between 9 and 4 k ^{14}C a BP suggested that the northern boundary of the Asian summer monsoon reached the BJD and brought higher precipitation to the Gobi region at this time (Yang, 2000; Yang et al., 2003). One root-shaped nodule and three calcareous root tubes from a megadune in the desert were radiocarbon dated to ~4.4–27.9 k ^{14}C a BP and another two samples, travertine from modern lake and calcareous root tubes from limnic relics, were dated to ~8.5 and ~8.4 k ^{14}C a BP, respectively (Chen et al., 2004b). The frequencies in ^{14}C ages of the calcareous root tubes were interpreted as a proxy of effective moisture on the millennial scale (Li et al., 2015b, 2015c). The results revealed that ~62% of the Holocene samples were dated to 7–5 Cal ka BP and ~38% were dated to 4–2 Cal ka BP over the Alxa Plateau, while in the BJD all Holocene samples were dated to 7–5 Cal ka BP (Li et al., 2015c). In a study of megadune growth patterns based on optically stimulated luminescence (OSL) ages of wet sand layers in the dune hills, Liu et al. (2016) proposed that main megadune growth periods took place in humid climate, when water acted as a cementing agent in dune construction. Several studies have suggested that lakes in and adjacent to the study area expanded during the Holocene, based on ^{14}C dating of various materials from interdune palaeolake sediments (Yang and Williams, 2003,Yang et al., 2003, 2010, 2011; Yang and Scuderi, 2010; Hartmann and Wünnemann, 2009; Li et al., 2010; Wang et al., 2016a). OSL dating of lacustrine sediments demonstrated the existence of lakes during MIS5 (Bai et al., 2011; Fan et al., 2014), while a drill core from the eastern shore of Lake Xinuoertu, a salt lake in the centre of the BJD, suggests that the area was lake dominated during MIS5, but with increased aeolian activity (Wang et al., 2015).

Previous studies in the BJD have shown that the area experienced dramatic environmental changes during the Late Quaternary. However, the interdune lake evolution in the BJD remains unknown, partly because the strong wind erosion has resulted in gaps in the sedimentary records and the scattered interdune lake basins were also strongly influenced by the fast migration of the sands around the lake basins. Additionally, most of the reported chronologies have used ^{14}C dating as the primary dating method, which is only useful for deposits younger than ~45 ka (Pigati et al., 2007), even only useful within ~20 ka when using inorganic materials from arid areas in which case ages older than 25 ka are saturated (Lai et al., 2014; Song et al., 2015). The other reported chronologies rarely cover MIS5 and are also limited and unsystematic (Fig. 1). The situation of limited age control hinders the understanding of the evolution and palaeoenvironmental significance of interdune lakes in the BJD. This study provides a chronology of lacustrine sediments, based on 21 ages from seven profiles in lake shorelines and limnic relics, which allows a more systematic and nuanced analysis of their palaeoenvironmental significance and evolution in the Late Pleistocene.

2. Geological and physiographical setting

The BJD lies on the western part of the Alxa Plateau in northern China, covering an area of ca. 5.22 × 10^4 km^2 (Zhu et al., 2010). The BJD is surrounded by mountains on three sides (Fig. 2), with the Heli, Beida and Longshou mountains to the south and the Zongnai Mountains to the east. In the southeast, the Yabulai Mountains separate the Badain Jaran from the Tengger Desert. To the west and north is the alluvial/lacustrine plain formed by the Heihe River in which Gurinai Oasis located (Wang et al., 2015). The elevation of the BJD gradually decreases from approximately 1800 m in the southeast to 1000 m in the northwest (Dong et al., 2004). Lying at the northwestern range of the East Asian Summer Monsoon (EASM), the region is characterized by the typical arid landscape of the monsoon–westerly wind transitional zone (Chen

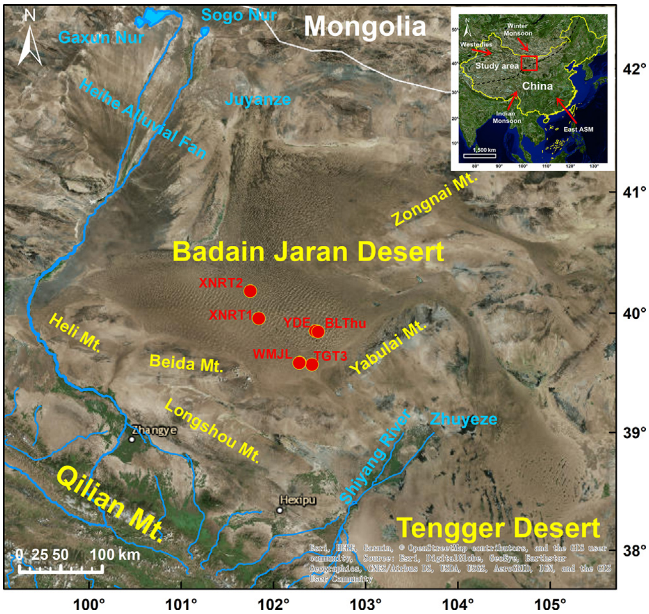

Fig. 2. Location maps. Geographic setting of the study area and the location of sampling profiles, cities/towns and geomorphological features mentioned in the text. The modern Asian summer monsoon limit (black dashed line at inset) is summarized from Chen et al. (2010, 2018), Wang et al. (2017), and Li et al. (2018b).

et al., 2003), and is sensitive to climate change. At the present day, the climate of the BJD is classified as extreme continental, with cold winters and very low precipitation (< 90 mm, mainly falling from June to August and decreasing from the southeast to the northwest). Annual potential evaporation (> 2500 mm) and mean annual temperature (9.5–10.3 °C) increase from south to north as elevation decreases. Mean annual wind speed, which ranges from 2.8 to 4.6 m s^{-1}, also increases from south to north, with the strongest winds in April and May (Dong et al., 2004). Based on a modified Penman Equation approach, combined with weather data from CE 1961 to 2001 from the margins, Yang et al. (2010) re-estimated the mean annual evaporation from lake surfaces and dune slopes in the BJD, and suggested that the mean annual evaporation is ca. 1040 mm from the lake surface and ca. 100 mm from land surfaces in the southeastern part of the desert. Both of the values are much lower than previously published in literature. The dominant winds are from the northwest, northeast, and southwest (Zhang et al., 2015).

The BJD is known for the highest megadunes in the world and its unique alternating megadune–lake landscape. Dong et al. (2004) estimated that over 60% of the desert is occupied by megadunes, of which 42.1% are > 300 m high, 38.2% between 200 and 300 m and 19.7% < 200 m. The primary dune types are compound transverse and compound star (Dong et al., 2004). The tallest megadune, Bilutu Peak, is a compound transverse dune with a height of ~450 m (Liu et al., 2016). Currently there are more than 100 lakes in the BJD (Zhu et al., 1980; Yang et al., 2010; Wang et al., 2016a), with a total area of about 22.30 km^2 including six exceeding 1 km^2 and 46 between 0.1 and 1 km^2 (Yang et al., 2010). Most of the lakes are concentrated in the southeast of the desert (Fig. 2). The interdune depressions contain a large number of seepage lakes with no surface runoff, which vary considerably in terms of area and salinity (Hofmann, 1996; Yang and Williams, 2003).

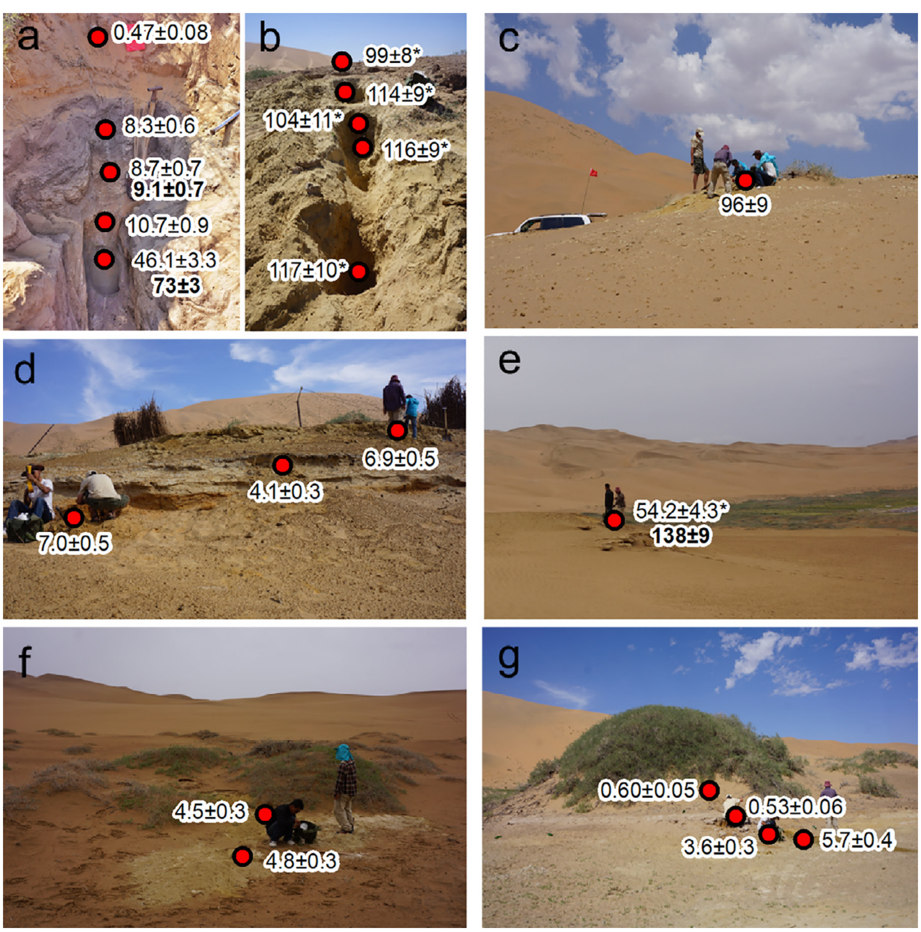

Fig. 3. Photographs of study profiles, demonstrating typical appearances of aeolian sand, gyttja and lacustrine sediment relics, as well as sampling positions. (a) Yindeertu Playa (YDE); (b) Tonggutu Playa (TGT3); (c) Bilutu Playa (BLThu); (d) Womenjilin Playa (WMJL2); (e) Xinuoertu Playa (XNRT2); (f) Xinuoertu Playa (XNRT1); (g) Womenjilin Playa (WMJL1).

3. Profiles and luminescence dating sampling

For this study, detailed ground survey and luminescence dating sampling was conducted over a three-year period in the southeastern BJD (Fig. 2). This area was chosen for study as it is where the highest concentration of lakes occurs. The main types of sediment in the southeastern desert include aeolian, sinter, gyttja and lacustrine. Field observations and interpretation of shorelines in ETM^+ imagery by Yang et al. (2010) showed the areas of lake surface have been significantly expanded in the past, and some completely desiccated at present. We sampled sediments associated with past lakes, found on palaeoshorelines and in dry lake basins, to provide evidence of paleoenvironmental changes. 21 luminescence samples were collected from seven sections from different lake basins to provide a systematic chronology (Fig. 3).

The Yindeertu Lake (YDE) section (Fig. 3a) was located at the east shoreline of the lake, in the southeastern BJD (Fig. 2), which covers an area of 1.57 km^2. The YDE section mainly comprises of aeolian vegetated sand dune, dark brown swamp (gyttja) and caesious lacustrine sediments (Fig. 6). The Tonggutu playa (TGT) section (Figs. 3b and 6) was located on a quasi-sinter platform of the playa, near the southern edge of the BJD (Fig. 2). The section is mainly composed of sinter (covered on the top) and lacustrine sediments. Sections WMJL-1 and WMJL-2 are located at Womenjilin playa (Fig. 2). The WMJL-1 section (Fig. 3g) is mainly composed of vegetated dune sand and lacustrine sediments (Fig. 6). The WMJL-2 section (Fig. 3d) is mainly composed of lacustrine sediments (Fig. 6). Sections XNRT-1 and XNRT-2 are located in the east of Xinuoertu playa (Fig. 2). Section XNRT-1 (Fig. 3f) comprised sinters overlying alternating caliche and lacustrine sediments. Section XNRT-2 (Fig. 3e) was located about 50 m above water level and the OSL sample was obtained from well-cemented lacustrine sediment at a depth of 30 cm (Fig. 6). The BLT section (Fig. 3c) was located northwest of Bilutu Lake, which is separated from Yindeertu Lake by Bilutu Peak (Fig. 2) and mainly composed of caesious lacustrine sediment with some rusty stripes (Fig. 6). More detailed information of all the aforementioned sections and the sampling depths in each section are listed in Table 1 and shown in Fig. 6. Large and clear figures for each section in Fig. 3 are provided online as supplementary materials (Figs. S1–S7).

All samples were collected by hammering steel tubes into freshly cleaned vertical sections (dug to a depth of original sediments). The tubes were then covered with aluminium foil, sealed with opaque tape and wrapped with a black plastic bag to avoid light exposure.

4. Luminescence dating

4.1. Sample preparation and measurement techniques

In the luminescence dating laboratory of Qinghai Institute of Salt Lakes, Chinese Academy of Sciences, the unexposed middle part of each OSL tube was used to extract quartz and potassium feldspar (K-feldspar) for equivalent dose (D_e) determination under red light. Samples from the middle part of the tubes were treated with 10% HCl and 30% H_2O_2 to remove carbonates and organics, respectively. Grain-size fractions of 38–63 or 90–125 μm was extracted by wet sieving upon availability. Heavy liquids with densities of 2.62, 2.75, and 2.58 g/cm^3 were used to separate the quartz and K-feldspar for 90–125 μm fraction. The 38–63 μm fraction was etched by 35% H_2SiF_6 for about two weeks to remove feldspars (Lai and Wintle, 2006; Lai et al., 2007a; Roberts, 2007). The 90–125 μm fraction was treated with 40% HF for 45 min to remove feldspars and the alpha-irradiated outer layer (~10 μm). The treated quartz grains were washed with 10% HCl to remove fluoride precipitates. The purity of quartz grains was checked by infrared (830 nm) stimulation, and any samples with obvious infrared stimulated luminescence signals were retreated with H_2SiF_6 or HF to remove feldspar contamination and avoid D_e underestimation (Duller, 2003; Lai and Brückner, 2008). The pretreated grains were then mounted on the centre (~0.7 cm diameter) of stainless steel discs (~0.97 cm diameter) with silicone oil. Material at the tube ends was reserved for measurement of U, Th and K concentrations by neutron activation analysis in the China Institute of Atomic Energy in Beijing. The elemental concentrations were converted into an annual dose rate according to Aitken (1985). For the 36–63 μm grains, the alpha efficiency value was taken as 0.035 ± 0.003 (Lai et al., 2008). The cosmic ray dose rate was estimated for each sample as a function of depth, altitude and geomagnetic latitude (Prescott and Hutton, 1994). For K-feldspar dose rates, a K concentration of 12.5 ± 0.5% and Rb concentration of 400 ± 100 ppm was assumed (Huntley and Baril, 1997). A water content of 20 ± 5% was used to calculate ages for Holocene paleolake shoreline sediments given that a generally stable lake environment existed in most periods of the Holocene, based on a previous study in adjacent areas (Li et al., 2017). A water content of 15 ± 5% was used as the life-average water content for MIS5 and MIS3 limnic relic samples, given that a dry environment resulted in a reduced water content during the last glacial period (Li et al., 2017). For samples from current sand dunes, a water content of 10 ± 5% was used to calculate ages based on a previous megadune study (Liu et al., 2016). The dosimetry data for quartz OSL and K-feldspar pIRIR dating of all samples are shown in Table 2.

All the measurements were carried out on an automated Risø TL/OSL-DA-20 reader equipped with blue diodes (λ = 470 ± 20 nm) and IR diodes (λ = 830 nm). Luminescence was stimulated by blue LEDs at 130 °C for 40 s, and detected with a 7.5 mm thick U-340 filter (detection window 275–390 nm) in front of the photomultiplier tube.

4.2. Luminescence characteristics and D_e determination

Preheat plateau tests were conducted on samples YDE-2 (gyttja) and YDE-5 (lacustrine sediments), and a preheat plateau was clearly identified from 240 to 280 °C in both samples (Fig. 4a and d). Preheat was at 260 °C for 10 s for natural and regenerative doses, and second preheat was at 220 °C for 10 s for test doses. Signals of the first 0.64 s stimulation were integrated for growth curve construction after background subtraction (last 10 s).

The SAR-SGC method (Lai and Ou, 2013), a combination of SAR protocol (Murray and Wintle, 2000) and the Standard Growth Curve (SGC) method (Roberts and Duller, 2004; Lai, 2006; Lai et al., 2007a, 2007b; Yu and Lai, 2012), was employed to determine the equivalent

Table 1
The location and type of lithology of the seven sections.

Sections	Latitude	Longitude	Elevation (m)	Typing of section lithology	Above modern basin floor (a.m.b.f) (m)
YDE	39°50′57.9″	102°27′13.1″	1193	Shorelines around modern lake basin	20
BLThu	39°50′33.18″	102°29′01.98″	1211	Shorelines above modern lake basin	20
XNRT1	39°57′15.48″	101°50′22.26″	1160	Shorelines around modern lake basin	15
XNRT2	40°10′54.72″	101°44′48.06″	1160	Shorelines above modern lake basin	50
TGT3	39°34′9.42″	102°25′4.86″	1224	Quasi-sinter platform around shorelines of dried lake basin	15
WMJL2	39°57′15.48″	101°50′22.26″	1211	Shorelines around dried lake basin	3
WMJL1	39°35′9.9″	102°17′1.26″	1210	Dried lake basin	2

Table 2
Quartz OSL dating and K-pIRIR dating (italic) results for limnic relics from the Badain Jaran Desert. The minimum ages are marked with asterisk (*).

Sample ID	Elevation (m)	Depth (cm)	Grain size (μm)	K (%)	Th (ppm)	U (ppm)	Water content (%)	De (Gy)	Dose rate (Gy/ka)	Age (ka)
YDE-1	1193	35	90–125	1.51 ± 0.05	4.10 ± 0.14	1.13 ± 0.06	10 ± 5	0.96 ± 0.15	2.06 ± 0.14	0.47 ± 0.08
YDE-2	1193	75	90–125	1.54 ± 0.05	4.46 ± 0.16	1.48 ± 0.07	20 ± 5	15.90 ± 0.51	1.92 ± 0.13	8.30 ± 0.61
YDE-3	1193	110	90–125	1.72 ± 0.06	5.68 ± 0.19	1.20 ± 0.06	20 ± 5	17.92 ± 0.71	2.06 ± 0.14	8.72 ± 0.68
								22.38 ± 0.57	*2.45 ± 0.15*	*9.13 ± 0.66*
YDE-4	1193	160	90–125	1.58 ± 0.05	5.62 ± 0.19	1.50 ± 0.07	20 ± 5	21.18 ± 1.12	1.98 ± 0.13	10.67 ± 0.91
YDE-5	1193	205	90–125	1.55 ± 0.05	3.63 ± 0.13	3.17 ± 0.11	15 ± 5	106.03 ± 2.70	2.30 ± 0.15	46.13 ± 3.30
								197.48 ± 6.94	*2.69 ± 0.16*	*73.41 ± 2.62*
BLThu1-1	1211	30	90–125	1.31 ± 0.05	2.93 ± 0.13	1.29 ± 0.07	15 ± 5	166.51 ± 8.94	1.74 ± 0.12	95.45 ± 8.46
XNRT1-1	1160	100	38–63	1.74 ± 0.06	4.72 ± 0.17	7.01 ± 0.19	20 ± 5	16.44 ± 0.19	3.45 ± 0.24	4.76 ± 0.33
XNRT1-2	1160	30	38–63	2.05 ± 0.06	6.32 ± 0.21	4.73 ± 0.15	20 ± 5	14.85 ± 0.37	3.30 ± 0.23	4.50 ± 0.33
XNRT2-1	1160	25	38–63	1.54 ± 0.05	4.49 ± 0.16	4.86 ± 0.15	15 ± 5	163.38 ± 6.23	3.01 ± 0.21	54.21 ± 4.31*
			90–125					*487.05 ± 6.21*	*3.40 ± 0.16*	*137.47 ± 9.32*
TGT3-1	1224	200	90–125	1.56 ± 0.05	4.81 ± 0.16	2.61 ± 0.10	15 ± 5	264.64 ± 12.11	2.27 ± 0.15	116.83 ± 9.46*
TGT3-2	1224	130	90–125	1.56 ± 0.05	4.52 ± 0.16	2.57 ± 0.10	15 ± 5	261.90 ± 8.65	2.26 ± 0.15	115.77 ± 8.59*
TGT3-3	1224	110	90–125	1.55 ± 0.05	4.82 ± 0.16	2.08 ± 0.08	15 ± 5	226.49 ± 17.18	2.18 ± 0.15	103.90 ± 10.50*
TGT3-4	1224	88	90–125	1.50 ± 0.05	4.63 ± 0.16	2.19 ± 0.09	15 ± 5	245.82 ± 11.59	2.16 ± 0.14	113.91 ± 9.27*
TGT3-5	1224	70	90–125	1.28 ± 0.05	4.54 ± 0.16	2.80 ± 0.10	15 ± 5	207.64 ± 9.02	2.10 ± 0.14	98.76 ± 7.70*
WMJL2-1	1211	240	38–63	1.70 ± 0.05	4.76 ± 0.16	5.53 ± 0.15	20 ± 5	21.33 ± 0.30	3.04 ± 0.21	7.01 ± 0.50
WMJL2-2	1211	170	38–63	1.72 ± 0.06	5.20 ± 0.18	6.45 ± 0.17	20 ± 5	13.77 ± 0.29	3.32 ± 0.23	4.14 ± 0.30
WMJL2-3	1211	35	38–63	1.55 ± 0.05	4.54 ± 0.16	2.59 ± 0.10	20 ± 5	16.05 ± 0.38	2.32 ± 0.16	6.93 ± 0.51
WMJL1-1	1210	190	38–63	1.66 ± 0.06	5.36 ± 0.18	2.25 ± 0.09	20 ± 5	13.23 ± 0.34	2.32 ± 0.16	5.70 ± 0.43
WMJL1-2	1210	120	38–63	1.71 ± 0.06	4.13 ± 0.15	1.23 ± 0.06	20 ± 5	7.55 ± 0.22	2.07 ± 0.15	3.64 ± 0.28
WMJL1-3	1210	100	90–125	1.59 ± 0.05	4.91 ± 0.17	1.30 ± 0.07	20 ± 5	1.04 ± 0.10	1.94 ± 0.13	0.53 ± 0.06
WMJL1-4	1210	55	38–63	1.60 ± 0.05	4.20 ± 0.15	1.47 ± 0.07	10 ± 5	1.41 ± 0.06	2.34 ± 0.17	0.60 ± 0.05

dose (D_e). In this study, an individual SGC was constructed for each sample based on the average of the growth curves which were measured with the SAR protocol. Twelve aliquots were then measured to obtain the values of test-dose-corrected natural signals only, and each of the values was matched in the SGC to obtain a D_e. For all samples, the final D_e is the mean of all SAR D_es and SGC D_es. Fig. 5b and d show typical OSL decay curves for YDE-2 and YDE-5, respectively, which indicate that the OSL signals were from the fast component. Fig. 5a and c show the growth curves of samples YDE-2 and YDE-5, respectively.

Dose recovery tests (Murray and Wintle, 2003), which can validate the SAR procedure, were performed on samples YDE-2, and YDE-5, and six aliquots of each sample were tested. The ratios of the average measured dose (13.90 Gy and 97.84 Gy) to the given dose (14.90 Gy and 105.90 Gy) suggested that the SAR protocol is suitable for D_e determination in this study.

Recuperation was calculated by comparing the sensitivity-corrected OSL signal of 0 Gy to the sensitivity-corrected natural signal to check the thermo-transferred signals. In this study, recuperations for different preheat temperatures were less than 2% of the natural signal, which is negligible (Fig. 4c and f). The 'recycling ratio' was introduced to check

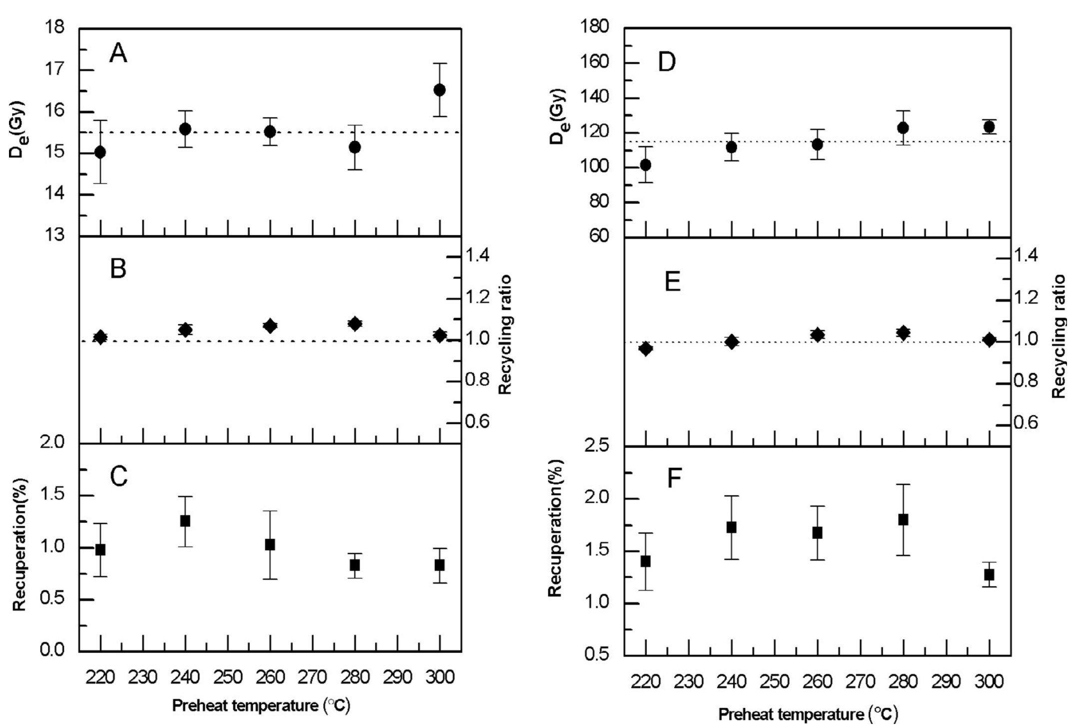

Fig. 4. Results of preheat plateau tests, recuperation and recycling ratio for YDE-2 (left) and YDE-5 (right). The equivalent dose (De) of each data point is the mean of four aliquots. The final chosen preheat temperature for quartz OSL dating in this study was 260 °C.

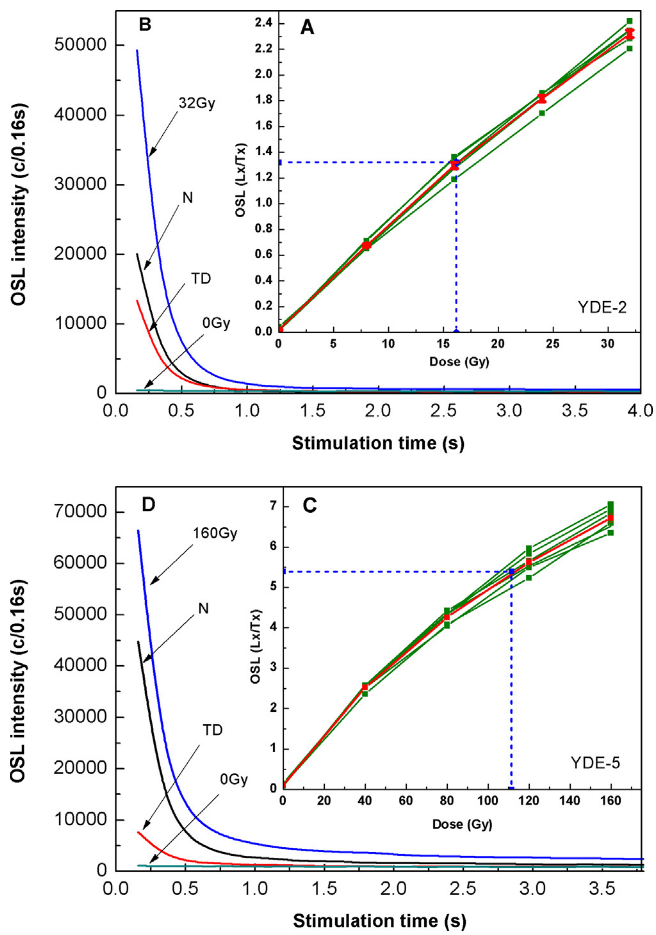

Fig. 5. Luminescence characteristics of sample YDE-2 (inset A and B) and YDE-5 (inset C and D). (B) and (D) display the decay curves for the natural (N) and regenerative doses of R3, 0 Gy and test dose (TD), respectively. (A) and (C) display the growth curves of six aliquots and the standard growth curve (SGC) (red lines), which is taken as the average of the six growth curves. The points (solid squares) defining each individual growth curve are depicted with error bars. The horizontal and vertical blue dashed lines indicate the projection of the average of sensitivity-corrected natural signals of the six aliquots onto the SGC.

for sensitivity change correction (Murray and Wintle, 2000), and for most aliquots, the recycling ratios fall into the acceptable range of 0.9–1.1 (Fig. 4b and e). The details of K-pIRIR dating were provided as supporting information (Appendix S1) due to the word limitation.

4.3. Dating results

Sample ages were obtained by dividing D_e by the dose rate. The calculated ages for all samples are listed in Table 2. The D_e values of samples from section TGT3 and XNRT2-1 are close to or larger than the $2D_0$ values (D_0 refers to the characteristic saturation dose). This means their quartz OSL ages are close to or beyond the saturation level. In order to avoid the underestimation and check the reliability of the chronologies, K-pIRIR dating was also applied on sample YDE-3, YDE-5 and XNRT2-1. We also tried to obtain the K-pIRIR ages of TGT3 section, but failed to exact enough K-feldspar to measure. As a result, the calculated quartz OSL ages are used as minimum ages for this section. The D_es of YDE-3 and YDE-5 are less than their $2D_0$ values, which representing unsaturated ages. The results showed that the quartz OSL age of sample YDE-3 is similar to the K-pIRIR age within the error, while the quartz OSL ages of sample YDE-5 and XNRT2-1 are younger than their K-pIRIR ages.

Although the OSL D_es of XNRT2-1 and BLThu1-1 are almost the same, their D_0 values are very different. The OSL D_e of BLThu1-1 (166.51 ± 8.94 Gy) is less than its $2D_0$ value (~240 Gy), while the OSL D_e of XNRT2-1(163.38 ± 6.23 Gy) is beyond the $2D_0$ value (~128 Gy). This is why the OSL age of XNRT2-1 was regarded as minimum, while the OSL age of BLThu1-1 was accepted and not regarded as minimum in the study. Consequently, the aforementioned reliable ages are used to discuss the environmental conditions.

As shown in Fig. 6, the ages of lacustrine sediments, gyttja and aeolian sediments in the BJD concentrate mainly in the early and middle Holocene and MIS5. In this study, only two samples were quartz OSL dated to MIS3. The quartz OSL age of XNRT2-1 is saturated and K-pIRIR dated to MIS5, while the quartz OSL age of YDE-5 is unsaturated and also K-pIRIR dated to MIS5. This severely limited our discussion about the paleoenvironment during MIS3 in the BJD. Thus, the paleoenvironment during MIS3 in the BJD still need further study.

5. Discussion

The occurrence of lacustrine and gyttja deposits in the YDE section (Fig. 3a) demonstrate that the area wetlands was much larger in the past, indicating a more humid environment in the region. The hiatus between caesious lacustrine sediments and dark brown gyttja implies an abrupt change in environmental conditions, which might be related to aeolian and lacustrine geomorphic dynamics. Drier conditions prevailed during the hiatus, leading to an increase in aeolian activity that not only terminated sedimentation in the section, but also initiated the wind erosion of previous sediments. The loss of material through erosion explains why the ages of 8.3 ± 0.6 ka and 73.4 ± 2.6 ka cannot represent the end time of the humid environment while the age of

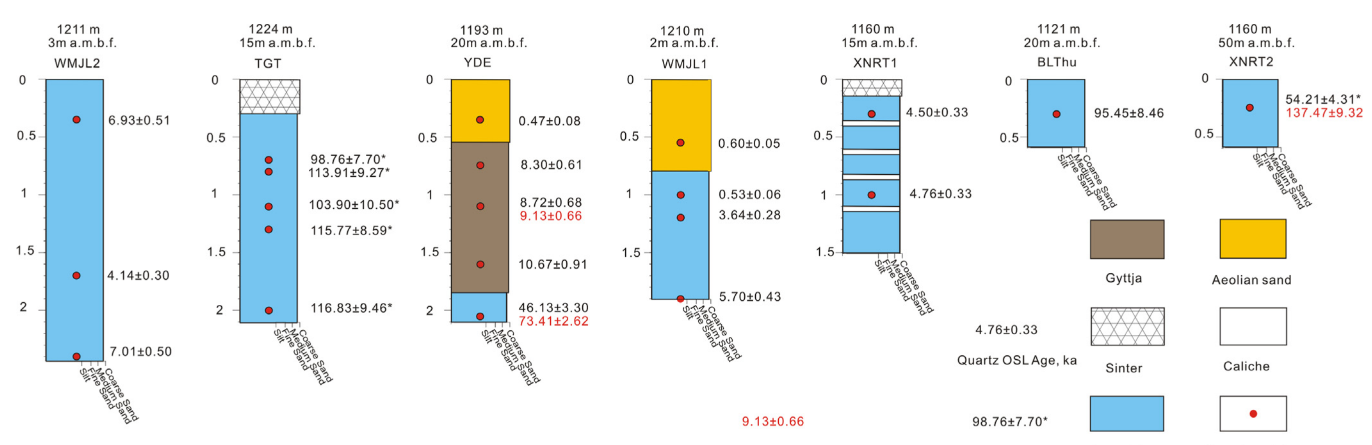

Fig. 6. Stratigraphy and ages of the seven studied profiles.

10.7 ± 0.9 ka can feasibly represent the start time of the humid environment (it also represents the end time of the dry environment). The age of 0.5 ± 0.1 ka, obtained from dune sand at the top of the section, represents the most recent activation of aeolian sand.

In sections WMJL and XNRT1 (Fig. 3c–e), the lacustrine chronology demonstrates that the two playas were much larger in area than today between 7.0 ± 0.5 to 3.6 ± 0.3 ka. The ages from lacustrine and gyttja deposits in the middle part of section YDE and sections WMJL and XNRT1 suggest that the BJD environment was humid during the early and middle Holocene (10.7 ± 1.0 to 3.6 ± 0.3 ka). The ages from the top part the YDE and WMJL1 sections (Fig. 3a and c), which is mainly composed of vegetated dunes or modern aeolian sediments, indicate high rates of aeolian activity during the last 600 years. The age of 0.5 ± 0.1 ka from the top of the lacustrine unit in the WMJL1 section (Fig. 6) was discarded as it was so close to the lacustrine surface that the luminescence signal was bleached by the sunshine and also mixed by the covered aeolian sand. This is roughly consistent with historical records within the Ejina Basin, which is near the BJD, was dry from the end of the Yuan Dynasty (1271–1368 CE) to the beginning of the Ming Dynasty (1368–1644 CE) (Liu, 1992), and also roughly consistent with the absence of shoreline features dating to younger than ~0.8 ka implies the Gaxun Nur paleolake dried up after ~0.8 ka, with only seasonal lakes remaining in the basin (Li et al., 2017). The high rates of aeolian activity during the last 600 years are also in accordance with the relatively dry periods revealed from a 2000 year geochemical record from the BJD (Ma et al., 2009).

Palaeolimnological relics indicative of a widespread humid paleoenvironment appeared in the desert. Usually the more weakly cemented materials on the margins of the lake are more easily eroded by wind, leaving the more well-cemented component in situ. Shorelines representing high lake levels associated with humid climate stages are preserved around current lakes and some were dated by luminescence. In section XNRT2, lacustrine terraces composed of silty-fine sand (Fig. 3e) represent a humid paleoenvironment around 137 ± 9 ka. Caesious lacustrine sediments at the bottom of the YDE section (Fig. 3a) formed before 73 ± 3 ka. Hence, the age shows that lacustrine sediments in sections XNRT2 and YDE were formed during MIS5 within error. The OSL ages of palaeolimnological relics in sections BLThu and TGT (Fig. 3g and b) show that the lacustrine sediments were formed at least between 117 ± 10 to 96 ± 9 ka, corresponding to MIS5. Although one age from the bottom of YDE section is problematic, the other ages from TGT, BLThu and XNRT2 sections reveal that at least some of the lacustrine sediments in the BJD formed during MIS5.

5.1. Holocene climate in the BJD

A number of studies published in the last decade or so have shed light on the Holocene environment of the BJD. The findings of Yang and Scuderi (2010), based on a radiocarbon chronology of interdune lacustrine deposits, showed that the high lake levels in the basins of the BJD indicate higher moisture availability during the middle Holocene (8–4 Cal ka BP), followed by a drier late Holocene. A more recent study of interdune lake relics by Wang et al. (2016a) demonstrated that while many lakes reached their maximum water level in the middle Holocene between 8.6 and 6.3 Cal ka BP, there was also expansion of lakes during the early Holocene, with limnic peat dated to between 11 and 10 Cal ka BP, and lake retreat or desiccation about 3.5–0 Cal ka BP. In an analysis of a 310 m drill core obtained from the desert centre, Wang et al. (2015) suggested that lacustrine material in the upper part of the core represented lake re-appearance during the warm and humid Holocene climate. However, research in the north of the BJD by Chen et al. (2003), based on the radiocarbon chronology of a core from Juyanze Lake, shows a more complicated picture, with a distinct mid Holocene drought between 7 and 5 Cal ka BP and two periods of lake expansion at 7 and 5–3 Cal ka BP. Hydrological changes in the eastern Juyanze basin reflect reconstructed Holocene climate history, with wet alternations in the early Holocene (10.7–7.6 Cal ka BP), dry phases in the mid Holocene (7.6–5.4 Cal ka BP) and wet conditions in the mid to late Holocene (5.4–1.5 Cal ka BP) (Hartmann and Wünnemann, 2009). The frequency of calcareous root tubes ^{14}C dating results were interpreted on the millennial scale as a proxy for effective moisture, and the frequency of the ^{14}C dating results reveal that all Holocene samples, from the Badain Jaran Desert, were dated to 7–5 Cal ka BP (Li et al., 2015b, 2015c). However, climate reconstructions from south of the BJD show a different pattern. A radiocarbon chronology from Zhuyeze suggests that the early Holocene (11.0–7.4 Cal ka BP) was relatively arid, a humid environment prevailed during the mid Holocene (7.4–4.7 Cal ka BP), while arid conditions prevailed again during the late Holocene (4.7–0 Cal ka BP) (Li et al., 2009). These findings are supported by an OSL chronology from Zhuyeze, Long et al. (2012), which also shows a warm and dry early Holocene (9.5–7.0 ka), cool and humid mid Holocene (7.0–4.8 ka), and an increasingly arid late Holocene (since 4.8 ka). A radiocarbon chronology and other indexes from loess stratigraphy at Chagelebulu, on the southern fringe of the Badain Jaran (Gao et al., 2006) also confirm the overall trends, with loess accumulation between 9.4 and 8.2 Cal ka BP and 7.2–4.3 Cal ka BP, and palaeosol development between 3.3 and 2.2 Cal ka BP.

Although there is broad agreement between the above studies, the precise timing of the initiation and termination of each climatic stage varies between different dating methods and indexes of geochemistry in different sections. In this study, the age of YDE-4 in the YDE section indicates humid environment initiation at 10.67 ka and continuation during the early Holocene (10.7 ± 1.0 to 8.3 ± 0.6 ka). The youngest lacustrine sediment, in section WNJL1, implies the termination of aridity in the BJD around 3.6 ± 0.3 ka. In summary, this study shows that environment in the BJD was humid in the early and middle Holocene (10.7 ± 1.0 to 3.6 ± 0.3 ka), with aridity prior to 10.7 ka and since 3.6 ka, respectively.

In a synthesis of literatures published prior to the early 1990s, Shi et al. (1993) concluded that both the temperature and precipitation were high in China between 8.5 and 3.0 ka. However, An et al. (1993 and 2000) argued that effective precipitation peaked at 9 Cal ka BP in monsoon areas of northern and northwestern China, and that precipitation declined and aridity increased thereafter. In a study of the western part of the Chinese Loess Plateau, An et al. (2003) showed that wetland/swamp layers formed between 9.0 and 3.8 Cal ka BP, indicating a humid climate in that period. A pollen-based, well-dated ~20-yr-resolution quantitative precipitation reconstruction from an alpine lake on the Central Loess Plateau provide a robust EASM variation records since last deglaciation, which clearly showed humid in mid-Holocene (7.8–5.3 ka), relative humid in early Holocene (14.7–7.0 ka), and dry in late Holocene (since ~3.3 ka) in monsoonal East Asia (Chen et al., 2015). A study of loess and aeolian sand from the eastern Qaidam Basin also indicates a humid climate between 8.0 and 4.5 ka and relative aridity between 4.5 and 0.5 ka (Yu and Lai, 2012). The aeolian signature from lacustrine sediments of the Qaidam Basin in northeastern Qinghai-Tibetan Plateau indicates that extremely arid and relative shallow-water environment ended at about 12.5 ka (An et al., 2012). It is plausible that the climate during the early and middle Holocene (10.7–3.6 ka) was humid even in the transition zone of the Westerlies and the East Asian monsoon. In summary, the luminescence ages of lacustrine sediments in the BJD reported in this study are consistent with the general trends of reported Holocene monsoon variations in east and south Asia. This would also be consistent with the Holocene high lake levels and pan-lake period in the BJD reported by Wang et al. (2016a). Minor differences in the chronologies of the gyttja layers may be attributed to the floating interdune lake basin and the different dating methods.

5.2. Late Pleistocene climate in the BJD

Most previous work on the climate of the BJD has focused on the

Holocene (Yang and Williams, 2003; Yang et al., 2003, 2010, 2011; Hartmann and Wünnemann, 2009; Li et al., 2010; Wang et al., 2016a) and only a few lacustrine chronologies prior to the Holocene have been reported (Yang et al., 2003; Bai et al., 2011; Wang et al., 2011; Li et al., 2015b, 2015c; Fan et al., 2016). Earlier research on climate change in the BJD was constrained by the limits of conventional radiocarbon dating, with no ages older than MIS3 until the application of OSL and ESR dating methods. The Chagelebulu stratigraphic profile, in the southeastern part of the Badain Jaran sand sea, has been studied in detail and has been shown to contain a record of climate change since the Late Pleistocene (Gao et al., 1995, 1998, 2006; Dong et al., 1996; Li et al., 2005a, 2005b). A recent drill core (WED-02) from the BJD, dated by OSL and electron spin resonance (ESR), revealed that the area was lake dominated between 15 and 0 ka and from 130 to 70 ka, but the older period was subject to increased aeolian activity (Wang et al., 2015). Formation of lacustrine sediments in the BJD during MIS5 has also been reported by Bai et al. (2011) and Fan et al. (2014). A K-feldspar pIRIR dating study of Ejina Basin megalake, located in the north of the BJD, showed that megalakes formed prior to ~350 ka, and at ~320–310 ka, 240–180 ka, 120–80 ka, and ~5 ka, corresponding to > MIS 9, MIS 9, MIS 7, MIS 5 and the mid Holocene (MIS 1), respectively (Li et al., 2018a). A study of megadune evolution in the BJD showed the ages of wet sand layers to be concentrated in the early to middle Holocene and the last interglacial (corresponding to MIS 5e) (Liu et al., 2016). Similar chronologies of lacustrine sediments and paleolake shorelines, which represent humid climate during MIS5, have been reported from adjacent areas (Madsen et al., 2008; Fan et al., 2010; Liu et al., 2010, 2018; Li et al., 2015a, 2017; Xu et al., 2018). In this study, OSL chronologies for palaeolimnological relics corresponding to MIS5 also support a humid environment in the BJD from 138 ± 9 to 96 ± 9 ka. Hence, there is good supporting evidence for widespread humidity in northwestern China during MIS5.

Since the 1990s, different scholars have had divergent views on the formation and evolution of the unique megadune–lake landforms in the BJD (Dong et al., 2013). Climatic change has been regarded as one of the main contributing factors, particularly as the desert is located in the transition zone between the Asian summer monsoon and the Westerlies. Although the precise contribution of the two atmospheric systems in the BJD is still controversial, migration of the location of the transition zone is likely to have influenced effective moisture availability in the desert, and the enclosed interdune lakes could preserve such changes sensitively. Analysis of the limnic relics in our sections has revealed that the BJD environment has experienced several humid stages that are well preserved in the stratigraphic record. Due to wind erosion during dry phases, interdune lake basins have shifted in response to climate changes. This suggests that it is difficult to retrieve a long-term and continuous climate record from one lake basin. Hence, further studies of limnic relics and fossilized dunes elsewhere in the BJD are required to fully reveal the record of environment change and its influence on the formation and evolution of megadune–lake landforms.

6. Conclusions

This paper reports luminescence chronologies for limnic relics located in the core area of the BJD, which differ from most previous research in the region focusing on the desert margins and adjacent areas. Based on systematic geomorphological observations and luminescence dating, we established a primary chronological framework for interdune lake deposits and concluded that:

(1) Limnic relics of interdune lakes of the BJD can be used as a good record of environment change. However, the migration of the lake depocenter limited their potential as the long-term and continuous climate information archives.
(2) The BJD experienced a humid and lacustrine environment in the early and middle Holocene (10.7 ± 1.0 to 3.6 ± 0.3 ka), with arid condition prevailing immediately prior to 10.7 ka and since 3.6 ka. Aeolian processes have been more active during the last 600 years.
(3) Our luminescence chronologies from the limnic sediments suggest that the BJD had experienced a humid and lakes dominated environment during MIS5. Our data extends the dating results of previous ^{14}C chronologies from 30 to 40 ka in the desert to ages of 90–100 ka.

Acknowledgements

This work was funded by Chinese Academy of Geological Sciences (CAGS) Basal Research Fund Special Funds (Nos. YYWF201525, YYWF201618), the "Strategic Priority Research Program" of the Chinese Academy of Sciences (Climate Change: Carbon Budget and Relevant Issues, Grant No. XDA05120501), NSFC (Nos. 41571006 and 41761144073) and Natural Science Foundation of Shandong Province (ZR2015JL015). We are immensely benefited from the comments and suggestions by two anonymous reviewers. The authors also thank Dr. Xiangjun Liu for valuable suggestions while writing the manuscript.

Appendix A. Supplementary material

Supplementary data to this article can be found online at https://doi.org/10.1016/j.jseaes.2019.03.024.

References

Aitken, M.J., 1985. Thermoluminescence Dating. Academic Press, London, pp. 359.
An, C.B., Feng, Z.D., Tang, L.Y., 2003. Evidence of humid mid-Holocene in the western part of the Chinese Loess Plateau. Chinese Sci. Bull. 48 (22), 2472–2479.
An, F.Y., Ma, H.Z., Wei, H.C., Lai, Z.P., 2012. Distinguishing aeolian signature from lacustrine sediments of the Qaidam Basin in northeastern Qinghai-Tibetan Plateau and its palaeoclimatic implications. Aeolian Res. 4, 17–30.
An, Z.S., Porter, S.C., Kutzbach, J.E., Wu, X.H., Wang, S.M., Liu, X.D., Li, X.Q., Zhou, W.J., 2000. Asynchronous Holocene optimum of the East Asian monsoon. Quaternary Sci. Rev. 19, 743–762.
An, Z.S., Porter, S.C., Zhou, W.J., Lu, Y.C., Donahue, D.J., Head, M.J., Wu, X.H., Ren, J.Z., Zheng, H.B., 1993. Episode of strengthened summer monsoon climate of Younger Dryas age on the Loess Plateau of central China. Quaternary Sci. Rev. 39, 45–54.
Bai, Y., Wang, N.A., He, R.X., Li, J.M., Lai, Z.P., 2011. Ground penetrating radar images and optically stimulated luminescence dating for lacustrine deposition of the Badain Jaran Desert. J. Desert Res. 31 (4), 842–847 (in Chinese with English abstract).
Chen, F.H., Wu, W., Holmes, J.A., Madsen, D.B., Zhu, Y., Jin, M., Oviatt, C.G., 2003. A mid-Holocene drought interval as evidenced by lake desiccation in the Alashan Plateau, Inner Mongolia, China. Chinese Sci. Bull. 48 (14), 1401–1410.
Chen, F.H., Yu, Z.C., Yang, M.L., Ito, E., Wang, S.M., Madsen, D.B., Huang, X.Z., Zhao, Y., Sato, T., Birks, H.J.B., Boomer, I., Chen, J.H., An, C.B., Wünnemann, B., 2008. Holocene moisture evolution in arid central Asia and its out-of-phase relationship with Asian monsoon history. Quaternary Sci. Rev. 27, 351–364.
Chen, F.H., Chen, J.H., Holmes, J., Boomer, I., Austin, P., Gates, J.B., Wang, N.L., Brooks, S.J., Zhang, J.W., 2010. Moisture changes over the last millennium in arid central Asia: a review, synthesis and comparison with monsoon region. Quaternary Sci. Rev. 29, 1055–1068.
Chen, F.H., Xu, Q.H., Chen, J.H., Birks, H.J.B., Liu, J.B., Zhang, S.R., Jin, L.Y., An, C.B., Telford, R.J., Cao, X.Y., Wang, Z.L., Zhang, X.J., Selvaraj, K., Lu, H.Y., Li, Y.C., Zheng, Z., Wang, H.P., Zhou, A.F., Dong, G.H., Zhang, J.W., Huang, X.Z., Bloemendal, J., Rao, Z.G., 2015. East Asian summer monsoon precipitation variability since the last deglaciation. Sci. Reports 5, 11186.
Chen, J., Huang, W., Jin, L.Y., Chen, J.H., Chen, S.Q., Chen, F.H., 2018. A climatological northern boundary index for the East Asian summer monsoon and its interannual variability. Sci. China Earth Sci. 61, 13–22.
Chen, J.S., Li, L., Wang, J.Y., Barry, D.A., Sheng, X.F., Gu, W.Z., Zhao, X., Chen, L., 2004a. Ground-water maintains dune landscape. Nature 432, 459–460.
Chen, J.S., Zhao, X., Wang, J.Y., Gu, W.Z., Sheng, X.F., Su, Z.G., 2004b. Meaning of the discovery of lacustrine tufa and root-shaped nodule in Badain Jaran Desert for the study on lake recharge. Carsol Sin 23, 277–282 (in Chinese with English abstract).
Dong, G.R., Gao, Q.Z., Zou, X.Y., Li, B.S., Yan, M.C., 1996. Climatic changes on southern fringe of the Badain Jaran Desert since the Late Pleistocene. Chinese Sci. Bull. 41 (10), 837–842.
Dong, Z.B., Qian, G.Q., Lv, P., Hu, G.Y., 2013. Investigation of the sand sea with the tallest dunes on Earth: China's Badain Jaran Sand Sea. Earth-Sci. Rev. 120, 20–39.
Dong, Z.B., Wang, T., Wang, X.M., 2004. Geomorphology of the megadunes in the Badain Jaran Desert. Geomorphology 60, 191–203.
Duller, G.A.T., 2003. Distinguishing quartz and feldspar in single grain luminescence measurements. Radiat. Measur. 37, 161–165.
Fan, Q.S., Lai, Z.P., Long, H., Sun, Y.J., Liu, X.J., 2010. OSL chronology for lacustrine sediments recording high stands of Gahai lake in Qaidam basin, northeastern

Qinghai-Tibetan plateau. Quaternary Geochronol. 5 (2–3), 223–227.
Fan, X.L., Tian, M.Z., Liu, S.W., 2014. Environment evolution of the southeast Badain Jaran Desert during the last interglacial: evidences from grain size, OSL and 14C dating. Arid Land Geogr. 37 (5), 892–900 (in Chinese with English abstract).
Fan, Y.X., Zhang, F., Liu, W.H., Chen, X.H., Fan, T.L., Wang, Y.D., Chen, F.H., Lai, Z.P., 2016. History and mechanisms for the expansion of the Badain Jaran Desert, northern China since 20 ka: Geological and luminescence chronological evidence. The Holocene 26 (4), 532–548.
Gao, Q.Z., Tao, Z., Li, B.S., Jin, H.L., Zou, X.Y., Zhang, Y.C., Dong, G.R., 2006. Palaeomonsoon variability in the southern fringe of the Badain Jaran Desert, China, since 130 ka BP. Earth Surf. Process. Landforms 31, 265–283.
Gao, Q.Z., Dong, G.R., Li, B.S., Zou, X.Y., 1995. Evolution of southern fringe of Badain Jaran Desert since late Pleistocene. J. Desert Res. 15, 345–352 (in Chinese with English abstract).
Gao, Q.Z., Tao, Z., Dong, G.R., Li, B.S., Zou, X.Y., Su, Z., Jia, H.L., Yan, M.C., 1998. The characteristics of sediments geochemistry in Chagelebulu section in the Badain Jaran Desert. Supplement Acta Geogr. Sin. 53, 44–51 (in Chinese with English abstract).
Hartmann, K., Wünnemann, B., 2009. Hydrological changes and Holocene climate variations in NW China, inferred from lake sediments of Juyanze paleolake by factor analyses. Quaternary Int. 194 (1–2), 28–44.
Hofmann, J., 1996. Lakes in the SE part of Badain Jaran Shamo, their limnology and geochemistry. Geowissenschaften 14 (7–8), 275–278.
Huntley, D.J., Baril, M.R., 1997. The K content of the K-feldspars being measured in optical dating or in thermoluminescence dating. Ancient TL 15, 11–13.
Lai, Z.P., 2006. Testing the use of an OSL standardized growth curve (SGC) for De determination on quartz from the Chinese Loess Plateau. Radiat. Measur. 41, 9–16.
Lai, Z.P., Brückner, H., 2008. Effects of feldspar contamination on equivalent dose and the shape of growth curve for OSL of silt-sized quartz extracted from Chinese loess. Geochronometria 30, 49–53.
Lai, Z.P., Brückner, H., Zöller, L., Fülling, A., 2007a. Existence of a common growth curve for silt-sized quartz OSL of loess from different continents. Radiat. Measur. 42, 1432–1440.
Lai, Z.P., Mischke, S., Madsen, D., 2014. Paleoenvironmental implications of new OSL dates on the formation of the “Shell Bar” in the Qaidam Basin, northeastern Qinghai-Tibetan Plateau. J. Palaeolimnol. 51, 197–210.
Lai, Z.P., Ou, X.J., 2013. Basic procedures of optically stimulated luminescence (OSL) dating. Progr. Geogr. 32, 683–693 (in Chinese with English abstract).
Lai, Z.P., Wintle, A.G., 2006. Locating the boundary between the Pleistocene and the Holocene in Chinese loess using luminescence. The Holocene 16, 893–899.
Lai, Z.P., Wintle, A.G., Thomas, D.S.G., 2007b. Rates of dust deposition between 50 ka and 20 ka revealed by OSL dating at Yuanbao on the Chinese Loess Plateau. Palaeogeogr., Palaeoclimatol., Palaeoecol. 248, 431–439.
Lai, Z.P., Zöller, L., Fuchs, M., Brückner, H., 2008. Alpha efficiency determination for OSL of quartz extracted from Chinese loess. Radiat. Measur. 43, 767–770.
Li, B.S., Gao, Q.Z., Yan, M.C., Li, Y.Z., Dong, G.R., Wen, X.H., 2005a. A recent study on sedimentary sequence of southeastern Badain Jaran Desert since 150 ka BP. J. Desert Res. 25, 457–464 (in Chinese with English abstract).
Li, B.S., Hofmann, J., Chen, D.N., Wen, X.H., Yan, M.C., Zhang, D.D., Niu, D.F., Li, Z.W., Qiu, S.P., Wang, F.N., Du, S.H., 2010. A bio-stratigraphy evidence of summer monsoon drift on a large scale toward NW China during the Holocene Mega-thermal. J. Earth Environ. 1 (2), 133–138 (in Chinese with English abstract).
Li, G.Q., Jin, M., Duan, Y.W., Madsen, D.B., Li, F.L., Yang, L.P., Wei, H.T., Chen, F.H., 2015a. Quartz and k-feldspar luminescence dating of a Marine Isotope Stage 5 megalake in the Juyanze Basin, central Gobi Desert, China. Palaeogeogr., Palaeoclimatol., Palaeoecol. 440, 96–109.
Li, G.Q., Li, F.L., Jin, M., She, L.L., Duan, Y.W., Madsen, D., Wang, L.B., Chen, F.H., 2017. Late quaternary lake evolution in the Gaxun Nur Basin, central Gobi Desert, China, based on quartz OSL and K-feldspar pIRIR dating of paleoshorelines. J. Quaternary Sci. 32 (3), 347–361.
Li, G.Q., Chen, F.H., Xia, D.S., He, Y., Zhang, X.J., Madsen, D.B., Oldknow, C., Wei, H.T., Rao, Z.G., Qiang, M.R., 2018a. A Tianshan Mountains loess-paleosol sequence indicates anti-phase climatic variations in arid central Asia and in East Asia. Earth Planet. Sci. Lett. 494, 153–163.
Li, G.Q., Madsen, D.B., Jin, M., Stevens, T., Tao, S.X., She, L.L., Yang, L.P., Li, F.L., Wei, H.T., Duan, Y.W., Chen, F.H., 2018b. Orbital scale lake evolution in the Ejina Basin, central Gobi Desert, China revealed by K-feldspar luminescence dating of paleolake shoreline features. Quaternary Int. 482, 109–121.
Li, Y., Wang, N.A., Cheng, H.Y., Long, H., Zhao, Q., 2009. Holocene environmental change in the marginal area of the Asian monsoon: a record from Zhuye Lake, NW China. Boreas 38 (2), 349–361.
Li, Y.Z., Li, B.S., Gao, Q.Z., Jin, H.L., 2005b. Fluctuations of main chemical elements since 150 ka BP as indicated in Chagelebulu stratigraphical section, Badain Jaran Desert. J. Desert Res. 25, 8–14 (in Chinese with English abstract).
Li, Z.L., Wang, N.A., Cheng, H.Y., Ning, K., Zhao, L.Q., Li, R.L., 2015b. Formation and environmental significance of late Quaternary calcareous root tubes in the deserts of the Alashan Plateau, northwest China. Quaternary Int. 372, 167–174.
Li, Z.L., Wang, N.A., Li, R.L., Ning, K., Cheng, H.Y., Zhao, L.Q., 2015c. Indication of millennial-scale moisture changes by the temporal distribution of Holocene calcareous root tubes in the deserts of the Alashan Plateau, Northwest China. Palaeogeogr., Palaeoclimatol., Palaeoecol. 440, 496–505.
Liu, S.W., Lai, Z.P., Wang, Y.X., Fan, X.L., Wang, L.L., Tian, M.Z., 2016. Growing pattern of mega-dunes in the Badain Jaran Desert in china revealed by luminescence ages. Quaternary Int. 410, 111–118.
Liu, X.J., Lai, Z.P., Fan, Q.S., Long, H., Sun, Y.J., 2010. Timing for high lake levels of Qinghai Lake in the Qinghai-Tibetan plateau since the Last Interglaciation based on quartz OSL dating. Quaternary Geochronol. 5 (2), 218–222.
Liu, X.J., Lai, Z.P., Madsen, D.B., Li, G.Q., Yu, L.P., Huang, C., Chen, F.H., 2018. Late Quaternary highstands of Qinghai Lake, Qinghai-Tibetan Plateau. Quaternary Sci. 38, 1166–1178 (in Chinese with English abstract).
Liu, Y.C., 1992. Evolution of the Juyan Lake. J. Arid Land Resour. Environ. 6, 9–18 (in Chinese with English abstract).
Long, H., Lai, Z.P., Fuchs, M., Zhang, J.R., Li, Y., 2012. Timing of late quaternary palaeolake evolution in tengger desert of northern china and its possible forcing mechanisms. Glob. Planet. Change 92–93, 119–129.
Lou, T.M., 1962. The formation and utilization of the desert between Minqing and Badain Monastery. Research of Desert Control, Series 3. Science Press, Beijing, pp. 90–95 (in Chinese).
Ma, J.Z., Edmunds, W.M., He, J.H., Jia, B., 2009. A 2000 year geochemical record of palaeoclimate and hydrology derived from dune sand moisture. Palaeogeogr., Palaeoclimatol., Palaeoecol. 276, 38–46.
Madsen, D.B., Ma, H.Z., David, R., Jeffrey, B.P., Forman, S.L., 2008. Age constraints on the late quaternary evolution of Qinghai Lake, Tibetan plateau. Quaternary Res. 69 (2), 316–325.
Murray, A.S., Wintle, A.G., 2000. Luminescence dating of quartz using an improved single-aliquot regenerative-dose protocol. Radiat. Measur. 32, 57–73.
Murray, A.S., Wintle, A.G., 2003. The single aliquot regenerative dose protocol: potential for improvements in reliability. Radiat. Measur. 37, 377–381.
Prescott, J.R., Hutton, J.T., 1994. Cosmic ray contributions to dose rates for luminescence and ESR dating: large depths and long-term time variations. Radiat. Measur. 23, 497–500.
Pigati, J.S., Quade, J., Wilson, J., Jull, A.J.T., Lifton, N.A., 2007. Development of low-background vacuum extraction and graphitization systems for ^{14}C dating of old (40–60 ka) samples. Quaternary Int. 166, 4–14.
Roberts, H.M., 2007. Assessing the effectiveness of the double-SAR protocol in isolating a luminescence signal dominated by quartz. Radiat. Measur. 42, 1627–1636.
Roberts, H.M., Duller, G.A.T., 2004. Standardised growth curves for optical dating of sediment using multiple-grain aliquots. Radiat. Measur. 38, 241–252.
Shi, Y.F., Kong, Z.C., Wang, S.M., Tang, L.Y., Wang, F.B., Yao, T.D., Zhao, X.T., Zhang, P.Y., Shi, S.H., 1993. Mid-Holocene climates and environments in China. Global Planet. Change 7, 219–233.
Song, Y.G., Lai, Z.P., Li, Y., Chen, T., Wang, Y.X., 2015. Comparison between luminescence and radiocarbon dating of late Quaternary loess from the Ili Basin in Central Asia. Quaternary Geochronol. 30, 405–410.
Sun, P.S., Sun, D.Q., 1964. The hydrological geology of the western Inner Mongolia. Research of Desert Control, Series 6. Science Press, Beijing, pp. 121–146 (in Chinese).
Tan, J.A., 1964. The types of deserts in the Alashan Plateau, Inner Mongolia. Geographical Collections, Series 8. Science Press, pp. 43–52 (in Chinese).
Wang, F., Sun, D.H., Chen, F.H., Bloemendal, J., Guo, F., Li, Z.J., Zhang, Y.B., Li, B.F., Wang, X., 2015. Formation and evolution of the Badain Jaran Desert, north china, as revealed by a drill core from the desert centre and by geological survey. Palaeogeogr., Palaeoclimatol., Palaeoecol. 426, 139–158.
Wang, L., Chen, W., Huang, G., Zeng, G., 2017. Changes of the transitional climate zone in East Asia: past and future. Climate Dyn. 49, 1463–1477.
Wang, N.A., Li, Z.L., Cheng, H.Y., Li, Y., Huang, Y.Z., 2011. High lake levels on Alxa Plateau during the Late Quaternary. Chinese Sci. Bull. 56, 1799–1808.
Wang, N.A., Ning, K., Li, Z.L., Wang, Y.X., Jia, P., Ma, L., 2016a. Holocene high lake-levels and pan-lake period on Badain Jaran Desert. Sci. China Earth Sci. 59 (1), 1–9.
Wang, T., 1990. Formation and evolution of Badain Jaran Sandy Desert, China. J. Desert Res. 10 (1), 29–40 (in Chinese with English abstract).
Wang, Z.T., Chen, T.Y., Liu, S.W., Lai, Z.P., 2016b. Aeolian origin of interdune lakes in the Badain Jaran Desert, China. Arabian J. Geosci. 9 (3), 190.
Xu, Y.T., Lai, Z.P., Chen, T.Y., Gong, S.L., 2018. Late Quaternary optically stimulated luminescence (OSL) chronology and environmental changes in the Hobq Desert, northern China. Quaternary Int. 470, 18–25.
Yan, M.C., Wang, G.Q., Dong, G.R., Li, B.S., 2001a. Study on mega dunes development and environmental change in Badain Jaran Desert. J. Desert Res. 21, 361–366 (in Chinese with English abstract).
Yan, M.C., Wang, G.Q., Li, B.S., Dong, G.R., 2001b. Formation and growth of high mega-dunes in Badain Jaran Desert. Acta Geogr. Sin. 56, 83–91 (In Chinese with English abstract).
Yan, M.C., Wang, G.Q., Li, B.S., Dong, G.R., 2001c. Pleistocene paleowind direction change in the Badain Jaran desert and its environmental significance. J. Tsinghua Univ. 41, 118–122 (in Chinese with English abstract).
Yang, X.P., 2000. Landscape evolution and precipitation changes in the Badain Jaran Desert during the last 30,000 years. Chinese Sci. Bull. 45 (11), 1042–1047.
Yang, X.P., 2001. Landscape evolution and paleoclimate in the deserts of northwestern China, with a special reference to Badain Jaran and Taklamakan. Chinese Sci. Bull. 46, 6–11.
Yang, X.P., Liu, T.S., Xiao, H.L., 2003. Evolution of megadunes and lakes in the Badain Jaran Desert, Inner Mongolia, China during the last 31,000 years. Quaternary Int. 104, 99–112.
Yang, X.P., Ma, N.N., Dong, J.F., Zhu, B.Q., Xu, B., Ma, Z.B., Liu, J.Q., 2010. Recharge to the inter-dune lakes and Holocene climatic changes in the Badain Jaran Desert, western China. Quaternary Res. 73, 10–19.
Yang, X.P., Scuderi, L., Paillou, P., Liu, Z.T., Li, H.W., Ren, X.Z., 2011. Quaternary environmental changes in the dry lands of China – a critical review. Quaternary Sci. Rev. 30, 3219–3233.
Yang, X.P., Scuderi, L.A., 2010. Hydrological and climatic changes in deserts of China since the late Pleistocene. Quaternary Res. 73, 1–9.
Yang, X.P., Williams, M.A.J., 2003. The ion chemistry of lakes and late Holocene desiccation in the Badain Jaran Desert, Inner Mongolia, China. Catena 51, 45–60.
Yu, L.P., Lai, Z.P., 2012. OSL chronology and palaeoclimatic implications of aeolian

sediments in the eastern Qaidam basin of the northeastern Qinghai-Tibetan Plateau. Palaeogeogr., Palaeoclimatol., Palaeoecol. 337–338 (4), 120–129.

Zhang, Z.C., Dong, Z.B., Li, C.X., 2015. Wind regime and sand transport in China's Badain Jaran Desert. Aeolian Res. 17, 1–13.

Zhu, J.F., Wang, N.A., Chen, H.B., Dong, C.Y., Zhang, H.A., 2010. Study on the Boundary and the Area of Badain Jaran Desert Based on Remote Sensing Imagery. Progr. Geogr. 29, 1087–1094 (in Chinese with English abstract).

Zhu, Z.D., Wu, Z., Liu, S., Di, X.M., 1980. Deserts in China. Science Press, Beijing 107 pp (in Chinese).